Electrostatic Rocket Exhaust Effects on Solar-Electric Spacecraft Subsystems

DAVID F. HALL* AND BRIAN E. NEWNAM†
TRW Systems Group, Redondo Beach, Calif.

AND

JAMES R. WOMACK‡
Jet Propulsion Laboratory, Pasadena, Calif.

Electrostatic rockets emit propellant particles into at least 2π sterad. Spacecraft designers therefore require tolerance-level criteria for the almost inevitable interception of propellant particles by spacecraft surfaces. A systematic analytical study was made of the possibly deleterious effects of Hg, Hg^+, Cs, and Cs^+ on spacecraft surfaces. Erosion of thin surfaces by sputtering, degradation of thermal control coatings, chemical degradation of nonmetallic surfaces, and condensation on solar cell cover glasses are expected to pose the most restrictive design constraints. Of these areas, quantitative constraints have been generated for condensation, assuming the initial existence of a monolayer of condensate. The others are at the qualitative stage and are under experimental study. Preliminary results are summarized. The application of the data developed is illustrated by calculation of Hg propellant condensation on the solar panels of a Jet Propulsion Laboratory (JPL) 1975 Jupiter flyby mission study.

Nomenclature

a = radius of exhaust plane
d = axial distance from rocket exhaust plane
E_D = desorption energy, ev
j = ion current density
k = Boltzmann's constant
m = molecular weight
n = atomic number density, atoms/cm^3
P = pressure
q = electronic charge
r = radial distance from center of rocket exhaust plane
R = solar distance, a.u.
S = sputtering yield: target atoms ejected per incident ion
t = time
T = temperature, °K
x = layer thickness
y = distance perpendicular to beam axis
α_s = solar absorptance
Γ = particle flux (particles cm^{-2} sec^{-1})
ϵ_H = hemispherical emittance
θ = angle from thrust vector
ρ = bulk resistivity
σ = Stefan-Boltzmann constant

Subscripts and superscripts

ar = arrival
b = back (dark) solar array surface
f = front (illuminated) solar array surface; also, final value
0 = initial value
+ = positive ion

Presented as Paper 69-271 at the AIAA 7th Electric Propulsion Conference, Williamsburg, Va., March 3–5, 1969; submitted March 24, 1969; revision received November 5, 1969. This work was performed for NASA and the Jet Propulsion Laboratory, California Institute of Technology, sponsored by NASA under contracts NAS 7-575 and NAS 7-100. The work of R. A. Meyers in chemistry, M. E. Kirkpatrick and R. A. Mendelson in metallurgy, and E. E. Luedke and L. R. Kelley in thermophysics sections is acknowledged.

* Member of the Technical Staff, Low Thrust Propulsion Department, Science and Technology Division. Member AIAA.
† Doctoral Candidate, University of Southern California.
‡ Engineer, Application Studies Group, Propulsion Research and Advanced Concepts Section.

Introduction

THE proposed use of solar-powered, electrically propelled vehicles for unmanned space exploration has been actively studied over the past few years. However, there are still questions which must be answered before this type of spacecraft can be utilized confidently. One is whether the use of mercury or cesium propellant in electrostatic thrusters might constrain the spacecraft (S/C) configuration, mission parameters, and/or thruster design. This question arises because of two considerations: 1) analyses and experimental data indicated that both electron bombardment (EB) and contact type thrusters emit particles into at least 2π sterad, and 2) most presently conceived solar-electric propulsion S/C require portions of some subsystems to occupy part of this 2π sterad volume.

The seeming inevitability of propellant interception by S/C subsystems indicates the need for increased knowledge on whether propellant arrival rates might degrade the performance of these subsystems. The propellant efflux from electrostatic thrusters consists of both ions and atoms. Therefore a systematic analytical study[1] was made of the possible deleterious effects of Hg, Hg^+, Cs and Cs^+ on S/C surfaces, and the results of this study are summarized here, along with recent preliminary experimental results. The potential deleterious interactions between the propellants and S/C components which have been identified are indicated in Table 1. Optical elements and coatings include solar cell cover glass and sensor lenses, and coatings thereon. The only problem areas not studied were those associated with moving joints and solid state components.

Electrostatic Rocket Exhaust

The primary ion beam of an electrostatic rocket is an approximately axisymmetric, geometrically expanding beam; ~94% of the beam is singly ionized atoms[2,3] with velocities of $\sim 3 \times 10^4$ m/sec, whose boundaries form angles of 15°–20° with the beam axis. For short-life cesium contact ionization rockets, ion current densities are presently between 10 and 20 ma/cm^2 at the exit plane with the possibility of

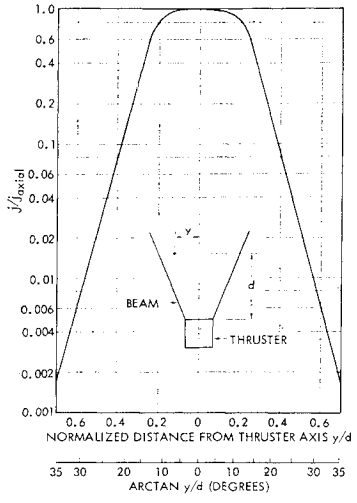

Fig. 1 Typical normalized ion current density distribution.

much higher densities in the future. Mercury and cesium EB rockets are operated in the 1–4 ma/cm² range.

Figure 1 conveys the general shape of the normalized ion current density distributions.[1,4] It should be emphasized that the ion current density distribution in the primary beam is a function not only of the electrical operating characteristics of the engine, but also of its mechanical design and fabrication tolerances. Since the distribution is important not only to the subject of exhaust effects on S/C surfaces but also to thruster efficiency and thrust vector precision, such data should be taken on all flight hardware thrusters.

The neutral atom efflux fraction ranges from ~1% in the Cs contact engines[5] to 10–20% for Hg EB thrusters.[6] This efflux has been experimentally shown[5] to follow approximately a cosine distribution for the Cs contact rocket (thermal velocity ~1400°K); the electrode geometry of EB rockets also leads to an approximately cosine distribution (thermal velocity ~500°K). Therefore, one may approximate the angular distribution of atoms from all circular engines by that of an extended cosine source

$$\Gamma(r,\theta) = \Gamma_0(a^2/r^2)\cos\theta[1 + (2a^2/r^2)\cos\theta + (a^4/r^4)]^{-1/2} \quad (1)$$

While Eq. (1) is not appropriate for all values (r,θ) with $r < a$, this restriction is of no consequence, because objects are not normally placed within one thruster radius of the exhaust plane. Reynolds[7] has discussed calculation of Γ_{ar} at arbitrarily located and oriented S/C surfaces, including those outside of line-of-sight to the thruster.

Ion engines also emit charge-exchange ions, i.e., particles which leave the primary ion production region as neutrals but subsequently undergo "near-miss" collisions with primary ions in which the original ion recombines with an electron from the neutral. The resulting particles are fast atoms with velocities (direction as well as speed) that the ions had at the time of collision, and slow ions which are subject to any electric fields present. If such collisions occur within the engine acceleration structure, these fields are large and divergent, producing a cone of ions surrounding the already extensive primary beam. If the collision occurs downstream of the neutralization plane (i.e., one or more inches downstream of the last engine accelerator plate), the ions will be accelerated normal to the beam boundary through a potential which is the difference between the beam plasma potential and the space potential outside the beam. This potential difference is typically less than 50 v.

The spatial and energy distributions of charge-exchange ions from a 15-cm-diam mercury EB engine have been studied with a hybrid computer technique by Staggs et al.[8] Unfortunately, computer limitations restricted calculations to $0 \leq \theta \leq 45°$, so that the distributions presented for $45° \leq \theta \leq 90°$ are educated guesses. Furthermore, these calculations are directly applicable only to the specific thruster studied. Therefore, at present, one can only estimate charge exchange ion arrival rates, and estimates for the most important range of angles will likely be the least accurate.

Some charge-exchange ions impact the thruster accelerator electrode producing an approximately cosine distribution of low vapor pressure metal. For instance, EB thrusters typically have approximately $1–3 \times 10^{-5}$ amp/cm² accelerator "drain" current density to a Mo electrode. The sputtering yield of polycrystalline Mo by 2 Kev Hg^+ is ~2.[9] Thus a Mo source flux of $\sim 2 \times 10^{14}$ atoms/cm²-sec exists.

Propellant Condensation Theory

Condensed layer formation proceeds in two stages: adsorption of propellant atoms on the S/C surface, followed by bulk condensation of atoms on this adsorbate. Desorption and then evaporation (or sublimation) compete with these processes in proportion to $\exp[-E_D/kT_s]$, where T_s is the surface temperature and E_D is the energy binding the atom to the surface. The value of E_D varies with surface composition and cleanliness, adsorbate species, and extent of adsorbate coverage. It affects whether the adsorbate forms as a uniform monolayer or as agglomerates. Usually its value is known precisely only for special substrates, such as atomically clean single crystals and the condensate itself.

Knowledge of the relative value of E_D for the atom-spacecraft surface combination ($E_D{}^0$) and the atom-condensate combination ($E_D{}^f$) is useful in predicting bulk condensation. When $E_D{}^0 > E_D{}^f$, adsorption will 1) be more or less uniform on the surface, and 2) occur and be sustained at lower Γ_{ar} and/or higher T_s than will subsequent condensation. Thus, condensation rates will be controlled by $E_D{}^f$. When $E_D{}^0 < E_D{}^f$, adsorption will 1) require higher Γ_{ar} and/or lower T_s than will subsequent condensation, and 2) proceed by a nucleation process often leading to macroscopic agglomerates. Thus, calculations based on $E_D{}^f$ will be "worst case," since the initial Γ_{ar} must exceed the equilibrium value at a given T_s. Langmuir[10] explains this "critical temperature" phenomenon by observing that if two adatoms are in contact, " . . . a larger amount of work must be done to evaporate one of these atoms than if the atoms were not in contact" and that the higher the arrival rate, the higher the probability that two or more adatoms will simultaneously occupy adjacent sites on the surface. Another means by which two or more adatoms may come into "contact" is through surface migration.[11] The kinetic energy an atom must acquire to migrate on a surface is typically much lower than the energy needed to leave it.

It is common laboratory experience that cesium wets most surfaces, a good indication of $E_D{}^0 > E_D{}^f$. According to

Table 1 Potential degradation of spacecraft components from impinging propellants

DEGRADATION MECHANISM ⇩ / SPACECRAFT COMPONENTS AFFECTED ⇨	THERMAL CONTROL COATINGS	OPTICAL ELEMENTS AND COATINGS	STRUCTURAL MATERIALS	INSULATORS AND ELECTRODE GAPS	CONDUCTORS	ADHESIVES	MOVING JOINTS	SOLID STATE COMPONENTS
PROPELLANT CONDENSATION AND/OR THRUSTER MATERIAL DEPOSITION	×	×		×				
CHEMICAL REACTION	×	×	×	×		×	×	
METALLURGICAL REACTION	×		×		×		×	
SPUTTERING EROSION	×	×	×	×	×	×	×	×
RADIATION DAMAGE (DEPOSITION OF ENERGY WITHIN SOLIDS, E.G. IONS)	×							×

× POTENTIAL PROBLEM AREA

Holland's review,[12] additional evidence for this relation may be found in the literature.

In contrast, it is common laboratory experience that mercury does not wet many surfaces, indicating $E_D{}^0 < E_D{}^f$. Glass is a notable and important example. Langmuir,[13,14] has discussed the experiments of R. W. Wood with mercury and cadmium on glass and his own cadmium experiments, in which condensation would not proceed at room temperature unless the surface had been previously cooled with liquid air to start the first monolayer.

Therefore, in the bulk layer growth analysis to follow, one may assume the presence of the initial cesium monolayer. In the case of mercury, the initial monolayer may not be formed without substantially exceeding the arrival rates necessary for subsequent layer growth, and the analysis is "worst case." However, in space, this worst-case condition may well exist because surface contamination may be removed by evaporation and ion sputtering, and insulating surfaces may become charged by impacting ions which may in turn enhance nucleation of droplets.

The bulk condensation of metals as a function of arrival rate and substrate temperature is readily predictable from kinetic theory and vapor pressure data, given an initial uniform coverage a few monolayers thick. Metallic vapors have unity sticking coefficient,[13,15] so if the neutral atom arrival rate exceeds the evaporation rate of the metal at a given sample temperature, bulk accumulation will proceed at a rate

$$dx/dt = [\Gamma_{ar} - P(T)(2\pi mkT)^{-1/2}]n^{-1} \qquad (2)$$

where n and T refer to the condensed layer, and $P(T)$ is its vapor pressure. If, on the other hand, the arrival rate is lower than the evaporation rate, only coverages of a few monolayers or less will result. At some locations in the exhaust the arrival rate of ions is a significant fraction of the total flux. Then it is necessary to calculate an effective Γ_{ar} which accounts for sputtering and ion condensation.

The diagonal lines of Fig. 2 are obtained from setting $dx/dt = 0$ in Eq. (2), inserting the appropriate values[16] for the two propellants of interest, and plotting Γ_{ar} vs $1000/T(°K)$. Therefore, these lines are the loci (Γ_{ar},T) which produce no change in condensed layer thickness. Above them, bulk accumulation proceeds. Below them condensed layer thickness decreases until approximately one monolayer

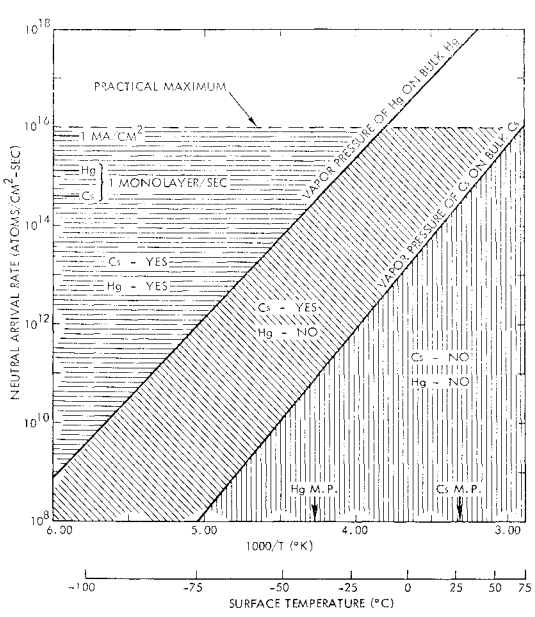

Fig. 2 Bulk accumulation regions for mercury and cesium atoms on surfaces where adsorbed monolayers already exist.

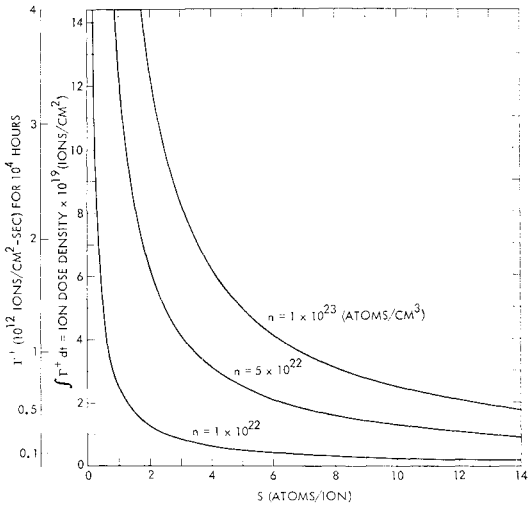

Fig. 3 Ion dose density required to produce 1-mil erosion vs sputtering yield for three target densities.

or less remains. It is seen that the region permitting bulk condensation of Cs is more extensive than for Hg. Note that in practice Γ_{ar} will not greatly exceed 10^{16} atoms/cm²-sec, which is approximately the neutral flux at the exit plane of a single thruster, and usually will be significantly lower. At 10^8 atoms/cm²-sec, $dx/dt \simeq 1$ monolayer/100 days in the absence of re-evaporation, so this is a practical lower limit of concern for bulk condensation effects.

Erosion, Chemical, and Metallurgical Effects

Spacecraft surfaces which intercept ions with kinetic energy in excess of ~25 ev may suffer erosion by sputtering. Both primary ions and most charge-exchange ions are of interest, but the latter are most likely to impose S/C design constraints because of their high-divergence angles. In present thrusters, charge-exchange ions have energies between 10 and 3000 ev. After an initial period during which the target becomes saturated with propellant atoms, the target erosion rate may be simply expressed

$$dx/dt = -\Gamma^+ S/n \qquad (3)$$

For a given target, S is a function of ion energy, ion species, and angle incidence. However, the angular dependence of S is approximately compensated by the reduction in projected target area so that eroded thickness is relatively independent of angle.

Thin surfaces, such as surface thermal coatings, will be the most sensitive to troublesome effects. Approximate values for S and n are available for metals[17] but are not generally available for nonmetals, especially organics. However, organics are expected to exhibit larger erosion rates than metals. Figure 3 indicates the integrated ion dose $\int\Gamma^+dt$ required to erode 1 mil (an example coating thickness; thicknesses range between 500 Å and 20 mils) vs S, with target density as the parameter. (Most materials fall between 10^{22} and 10^{23} atoms/cm³.) Ion dose is also expressed in terms of constant ion flux for 10^4 hr. It is seen that even fluxes below 10^{11} ions/cm²-sec may be troublesome. Erosion rates will be reduced in some cases by the arrival flux of propellant atoms[18] and target saturation effects,[19] and these effects require consideration in more detailed analysis.

Data on the chemical reaction between Hg or Cs and organic surfaces are sparse. Table 2 summarizes the results of literature search and analysis, and recent immersion tests. The analysis assumes an unlimited availability of propellant and the tests approximated this assumption; however, an ever-present adsorbed monolayer of propellant may well be equivalent to an unlimited supply. Chain scission results in

Table 2 Chemical effects of Cs, Cs^+, Hg, and Hg^+ on typical spacecraft materials

Material	Type	Extent of degradation[a] by Cs	Cs^+, Hg^+ [20]	CsOH[b, 21]	Hg[22]
H-Film[c]	Polyimide	Turns deep violet due to one electron oxidation-reduction (product probably highly conductive and photoconductive)[22]	(Moderate)[d]	(Severe hydrolysis with chain scission)	None
Teflon FEP[c]	Poly (perfluoroethylene propylene)	Turns black; C & CsF forms at surface[22]	(Severe, loss of fluorine)[d]	(None)	None
RTV 40	Amine cured silicone	(Little or none)[23]	(Moderate)[d]	(Moderate by hydrolysis)	(None)
Cat-a-lac black	Amine cured epoxy	(Little or none)	(Moderate)[d]	(Moderate)	(None)
PV-100	Silicone-alkyd resin; TiO_2 pigment	(Little or none of resin[23]; possible pigment dissolution)[24]	(Moderate, with darkening)[d]	(Moderate to severe due to hydrolysis)	(None)
Delrin[c]	Polyacetal	Little or none[22]	(Moderate)[e]	(None)	None
Sylgard 182[c]	Silicone	Little or none[22]	(Moderate)[d]	(Moderate)	None
SMRD 745[c]	Epoxy	Little or none[22]	(Moderate)[d]	(Little or none)	None
GT-100[c]	Polyester	Little or none[22]	(Moderate)[d]	(Slight to severe due to hydrolysis)	None
S-13	Methyl silicone + ZnO	(Little or none of resin[23] possible darkening of pigment)[24]	(Moderate, probable darkening due to pigment reaction)[e]	(Moderate)	(Slight or none)
Z-93	Potassium silicate + ZnO	(Slight at strain points,[25] moderate darkening)	(Moderate, with darkening)	(Moderate etching)	(Slight or none)
Al_2O_3		(Slight to moderate at strain points)[24-26]	(Slight)	(Slight etching)	(Slight or none)
BeO		(Slight to moderate at strain points)[24]	(Slight)	(Slight etching)	(Slight or none)
Corning 7740	Pyrex	(Slight to moderate at strain points)[25]	(Slight to none)	(Slight etching)	(Slight or none)
Corning 0211	Pyrex	(Slight to moderate at strain points)[25]	(Slight to none)	(Slight etching)	(Slight or none)

[a] Information in parentheses is postulated, based on analogous literature data; information without parentheses is data from literature and immersion tests.
[b] CsOH is anticipated when Cs arrives at surfaces having absorbed water vapor.
[c] Immersion tested in Cs and Hg for 48 hr.
[d] Surface chain degradation and cross-linking.
[e] Surface chain scission.

increased vapor pressure, while cross linking results in embrittlement. These results suggest that Hg^+ will be more troublesome than Hg^0, and that Cs will be of more concern than Hg. It is emphasized that these results are tentative; the comments within parentheses are postulated from literature data on analogous reactions. There is a clear need for further chemical experiments, and they are planned.

In considering metallurgical effects following propellant deposition, no distinction need be made between ions and neutrals. A search of the literature covering common S/C metals suggests that the most important metallurgical couples which could result in at least limited interactions were Cs/Au, Cs/solder, Hg/Au, Hg/Ag, and Hg/solder. Table 3 summarizes the results of this search. Quantitative data for the reaction kinetics of these couples were not found. Immersion of eutectic solder in both Cs and Hg resulted in heavy attack, and in Hg a marked decrease in ductility as well as decreased strength.[22] Less than one minute after application of a Hg surface coating to 7-mil-thick solder and Ag-Sn-Pb strips, they fractured easily.[22] In contrast, immersion of Ag in Hg for 4 weeks produced a 3-mil-deep reaction zone.[22]

Since metallurgical interactions must be preceded by the adsorption of propellant on the metal surface, minimum tolerable neutral arrival rates for surface effects may be deduced from adsorption and condensation phenomena. Arrival rates needed to produce bulk effects will be higher, since the propellant atoms must interact with the surface followed by diffusion into the bulk material. It is believed that several percent of propellant atoms in the bulk material would be required in most cases to cause serious bulk effects. However, surface reactions may increase thermal emittance, because the ϵ of metals is mainly proportional to $(\rho T)^{1/2}$ (Ref. 39). Although specific data on the couples of interest were not found, study of other alloys showed that large increases in resistivity occur from even limited alloying.

Effects of Ion Beam on Thermal Control Coatings

As previously discussed, the removal of coatings by sputtering will significantly affect S/C surface temperature. However, coatings may also be degraded by ion bombardment during their erosion lifetime, by such processes as changes in surface topography, the implantation of energy within the coating (radiation-type damage), and the chemical/metallurgical reaction of coating materials with implanted ions.[40-45] For some coatings the literature suggests qualitative trends regarding the functional dependence of degradation on ion energy, ion species, and ion dose. However, the information is incomplete; no references were found of experiments with Cs^+ or Hg^+, and most of the work reported was at relatively low ion energies. However, preliminary exposures[46] of various S/C coatings to very high fluxes ($\sim 10^{15}$ Hg^+/cm^2-sec) of 3kev Hg^+, resulting in large ion doses (6×10^{19} Hg^+/cm^2) have produced little change in any sample ϵ_H and in xenon simulated α_s of gold, Cat-a-lac black, 3M black, glass, and quartz. Marked changes were measured (*in situ*) in α_s of white paints (S13G, PV-100, Z-93) and in RTV-41 and RTV-566. Thus, one anticipates that unilluminated surfaces, where only ϵ_H is important, will be essentially free of thermophysical effects, while white paints may be among the most susceptible surfaces to rocket exhaust degradation.

Effects of Neutral Atom Propellant on Thermal Control Coatings and Solar Arrays

Thermal control coatings, including solar array surfaces, are also prominent targets for atom impingement. Performance degradation of these surfaces may result from optical properties of chemical/metallurgical reaction products which differ from those of propellant-free coatings or from the optical properties of condensed liquid metal films which differ from many coatings.

The subjects of the chemical and metallurgical reaction of the liquid metal propellants with thermal control coating materials are discussed in a previous subsection. Knowledge regarding these reactions and their rates, as well as the optical properties of the reaction products, is rather limited, and measurements are planned. Information does exist regarding optical properties and vapor pressures of the Cs and Hg. Therefore, it is possible to predict the surface thermal effects of atoms impinging on surfaces if it is assumed that there are no significant reaction products.

The optical properties of Cs and Hg used in the analysis appear in Table 4. (They were obtained by a careful review[1] of the experimental literature and available theories.) The solar absorptance of Hg is derived from the Zener-Drude free electron theory of metals,[47,48] which is in reasonable agreement with the best experimental data at 0.546μ. The solar absorptance of Cs is based on the data of Ives and Briggs[49] and Nathanson[50] over the 0.25 to 0.7μ range and an extrapolation of these data to longer wavelengths. The hemispherical emittances of both propellants are calculated from the theory of Parker and Abbott.[39]

Effects of Condensed Layers on Spacecraft Surfaces

Knowledge of the approximate values of the surface thermal properties of opaque mercury and cesium allows the following analytical description of the boundary conditions for, and rates of condensation of, these metals on various spacecraft surfaces. Only the effects of substituting these new surface thermal values for those of an uncontaminated spacecraft are considered. The Boeing Large Area Solar Array[51] has been chosen as a typical spacecraft surface undergoing atom impingement, but the analysis is fairly general, and the method is applicable to many other S/C surfaces.

Table 3 Metallic Interactions

Pair[a]	Interactions	Comments[b]
Ag-Hg	Ag dissolves to ~50 wt % Hg at S/C temperatures[30]	Probable B & S
Cu-Cs	Unknown-probably limited solubility[31]	Probably OK
Cu-Hg	Compound formed—limited solid solubility[27]	Probable S
Au-Cs	Compound formed—limited solid solubility[32]	Probable S
Au-Hg	Au dissolves to 20 wt % Hg, 2–3 compounds formed[33]	Probable B & S
Be-Cs	Be_2Cs is probable—no solubility data[29]	Experiment needed
Be-Hg	Be-Hg_2 is probable—room-temperature data suggests no amalgam[34]	B unlikely; S uncertain
Sn-Cs	Four compounds probable—limited solubility[35]	Probable S
Sn-Hg	1-2 compounds probable—measurable solubility is small[36]	Probable S
Pb-Cs	4-5 compounds possible with solid solubility of Cs in Pb of a few wt %[37]	Probable B & S
Pb-Hg	Hg-Pb_2 formed; 25 wt % solid solubility of Hg in Pb at S/C temperatures[38]	Probable B & S

[a] Pairs Al-Cs, Al-Hg, and Ag-Cs are OK; completely immiscible.[27-29]
[b] B = bulk effects; S = surface effects.

Table 4 Surface thermal properties of opaque Hg and Cs

	T, °K	State	ϵ_H	α_s
Hg	234	Solid	0.055	0.22 ± 0.05
	235	Liquid	0.10	0.22 ± 0.05
	248	Liquid	0.105	0.22 ± 0.05
	298	Liquid	0.12	0.22 ± 0.05
	373	Liquid	0.13	0.22 ± 0.05
Cs	248	Solid	0.02	0.25 ± 0.05
	301	Solid	0.03	0.25 ± 0.05
	302	Liquid	0.04	0.25 ± 0.05
	373	Liquid	0.05	0.25 ± 0.05

The first step is writing the heat balance equation for the array. It is assumed that the array has no lateral heat conduction, no radiant heat load other than that from the sun, no temperature gradient between its illuminated and dark surfaces and that the array is normal to the sun line and converts a negligible fraction of the solar energy into electrical energy. Then

$$T = \left[\frac{G(R)}{\sigma}\frac{\alpha_f}{\epsilon_f + \epsilon_b}\right]^{1/4} \tag{4}$$

where the solar flux $G(R)$ is 1400 $R^{-2}w/m^2$. Thus, array temperature depends on incident power density and the optical properties of its surface.

As shown in Fig. 2, the flux of arriving particles necessary to sustain a condensed layer is strongly dependent on the layer temperature. For the purposes of analysis these equilibrium curves may be expressed by

$$\log_{10}\Gamma_{ar} = -3.17(1000/T) + 28.16 \tag{5}$$

for mercury and by

$$\log_{10}\Gamma_{ar} = -3.73(1000/T) + 26.84 \tag{6}$$

for cesium. Substitution of Eq. (4) into Eq. (5) or (6) gives an expression for equilibrium condensation conditions on the array as a function of solar distance and array surface thermal properties. Four "boundary value" cases may be considered without further analysis. They are plotted in Fig. 4.

To obtain the "No Condensation" curves, the surface thermal values of the Boeing array are used: $\alpha_f = 0.78$, $\epsilon_f = 0.84$, $\epsilon_b = 0.88$. These curves represent the threshold values of Γ_{ar} for condensation. For smaller Γ_{ar}, condensation will not occur, because propellants re-evaporate as rapidly as they are supplied, but if Γ_{ar} exceeds these curves, some condensation will occur.

The curves labeled "Opaque Condensation on Front Surface" result from using propellant values for α_f and ϵ_f. They represent the equilibrium values of Γ_{ar} which result in constant thickness of an opaque propellant layer condensed on the solar cell side of the array. The formation of an opaque layer on the front surface of the array is ultimately a run-away process: these values of Γ_{ar} are smaller than the "No Condensation" values, because the array temperature is depressed by the presence of the propellant. Obviously, any portion of an array with such an opaque coating would not produce electricity.

The curves for "Opaque Condensation on Rear Surface" result from using propellant values for ϵ_b. Rather high equilibrium values of Γ_{ar} are required to sustain an opaque layer on the rear surface, because the array temperature is increased by the presence of the propellants. Furthermore, unless severe chemical/metallurgical reactions occur between the propellant and substrate, such a condensed layer would not be bothersome at 1 a.u. and beyond; the array temperature is always acceptably low (less than 400°K) at these distances.

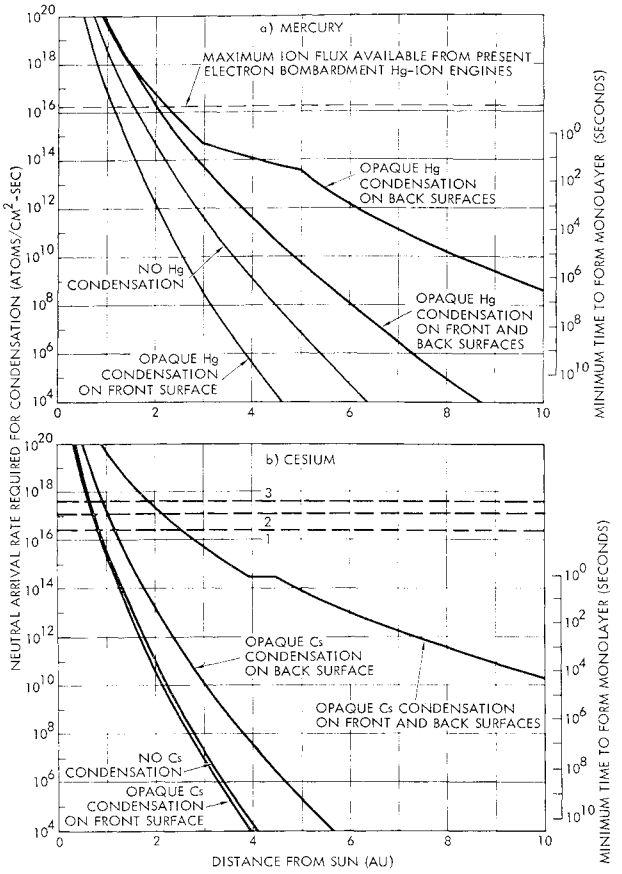

Fig. 4 Neutral mercury (a) and cesium (b) atom arrival rates necessary to sustain opaque condensation on Boeing solar cell array.

The curves for "Opaque Condensation on Front and Back Surfaces" result from using propellant values for α_f, ϵ_f and ϵ_b. Resulting equilibrium values of Γ_{ar} are very high, making this case academic.

The time scale for these events is roughly indicated by the right-hand scales on Fig. 4, which express the fact that a monolayer/cm² of mercury is $\sim 1.2 \times 10^{15}$ atoms; of cesium, $\sim 4 \times 10^{14}$ atoms. Carcful calculation of the time required to produce opacity must consider ϵ_H and α_s as a function of layer thickness and resulting re-evaporation rates during intermediate semitransparent stages, and layer transmission as a function of layer thickness and radiation wavelength.

Application

Using the spacecraft design and trajectory information from the results of a 1975 Jupiter Flyby Mission Study performed at the Jet Propulsion Laboratory,[25] an analysis was made to determine the neutral propellant arrival rates at various solar array locations. These results were then compared with the condensation calculations reported herein to illustrate the application of this information. This analysis indicates that near the end of the propulsion phase, some areas of the solar array may experience condensation on the illuminated surface. Therefore, additional analysis is needed to determine the propellant layer build-up rates and how these layers affect array performance through 1) the change in surface thermal properties and through attenuation of the light reaching the solar cells, and 2) chemical and metallurgical reactions. Further analysis is possible in these areas with presently available data; however, complete analysis would require additional data on Hg condensation anomalies, optical properties, and reaction rates.

The S/C and its mission have been described in a similar analysis by Reynolds.[7] Our results, shown as Fig. 5, are in general agreement, though displayed differently and based on the actual S/C configuration. The six numbered curves show the neutral arrival rates at six different points on one of the solar panels. Another of the panels receives an identical flux; the third and fourth receive none. The other three curves in Fig. 5 are segments of the Fig. 4a curves. The curves for locations 1 and 2 cross the "No Hg Condensation" curve at about 3.07 and 3.33 a. u. respectively (403 and 458 days). (Several other points in the neighborhood of location 1 were evaluated, and location 1 has the highest arrival rates of any point on the array.) Therefore, Hg may condense on the front surface of two of the inboard solar array panels.

To evaluate the extent of Hg condensation, several refinements and complicating factors must be considered: 1) the ranges in surface thermal properties of the array and the mercury; 2) heat radiations from the S/C and other sources to these locations; 3) layer growth, which will be proportional to the amount by which the arrival rate exceeds the re-evaporation rate, and the re-evaporation rate is a time-and-layer-thickness-dependent function of temperature§; 4) local cold spots, which might enlarge by lateral heat conduction through the array near the periphery of the spot; and 5) anomalous nucleation of mercury, or formation of the mercury layer as aggregates.[54] Thus, it is not possible to conclude, without further analysis, whether condensation will occur here. The excess mercury arrival rate is relatively small and occurs for a relatively short period. If the mission is to be undertaken, further analysis is warranted.

Electrical Effects

Electric rocket efflux striking S/C surfaces may reduce the resistance of electrical insulators or result in electrical breakdown. Two classes of increased insulator conductivity need be considered: that due to an adsorbed metallic layer on a chemically inert substrate, and that resulting from chemical reaction between metal atom and substrate. The former

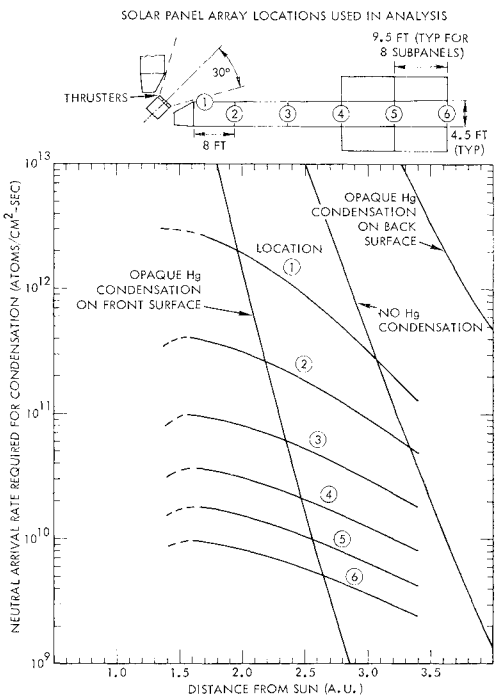

Fig. 5 Calculated mercury atom arrival rates at various solar array locations vs solar distance.

§ Uniform semitransparent films $\lesssim 10$ Å thick will raise T, because the front surface assumes the Hg value of ϵ more rapidly than it assumes the α value[53,54]; such an effect might increase the equilibrium value of Γ_{ar} by a factor of 3.

will be roughly proportional to layer thickness, with departures from this relation occurring for very thin layers when the so-called surface conductivity begins to replace the bulk conductivity of the liquid or frozen metal. The effects of electrical power dissipated in the layer must also be considered. Sufficient data are available to make these calculations. In contrast, calculation of increased conductivity due to chemical reaction between propellant and insulator is not possible at present. Knowledge of the chemical reactions between the metal atoms and organic insulators, and of the conductivity of reaction products, is tentative and incomplete. An experimental investigation of this problem is planned.

Another mechanism for electrical conduction across insulator surfaces is sliding sparks. A fractional monolayer of Cs on insulators (which may occur even in regions of the variables where bulk condensation is not permitted) provides a ready supply of electrons under strong field conditions giving rise to sliding sparks. Even dropwise condensation of Hg, which does not provide a continuous conduction path across insulators, affects this high voltage breakdown in both steady-state and transient conditions. Furthermore, many types of insulators deteriorate after sparking occurs.

The presence of propellant vapors within electrode gaps or the condensation of propellant on electrodes may lead to a variety of breakdown effects which temporarily or permanently damage spacecraft subsystems. Conditions permitting sustained electrical discharges across electrode gaps are not expected. Minimum breakdown in most gases and vapors occurs in the p-d range of 1–10 torr-mm. The equivalent pressure of propellant vapor fluxes of interest is less than 10^{-4} torr. Since spacings between electrodes will probably not exceed 1 m, it is clear that the normal condition will be one or more decades on the vacuum side of the Paschen minimum, and breakdown potentials will be at least a decade higher than the minimum, which is of the order of 300 v. Hence, breakdown through vapors represented by neutral efflux will not occur under normal conditions even for the high voltages used in the thruster.

Transient electrical breakdown could occur on some solar-electric missions. Sudden temperature increases of spacecraft surfaces associated with eclipse termination, vehicle reorientation, start-up of heat-generating equipment, or electrical arcs might desorb enough condensed propellant to raise propellant pressure momentarily into the 10^{-2} torr range. These effects are predictable from Paschen curve data given a specific spacecraft design and mission plan. High voltage (vacuum) arcs are a potential problem at thruster voltages. These arcs have received extensive study with clean[55,53] and cesiated[57] electrodes, from which adequate engineering calculations may be made.

Summary and Conclusions

Thin spacecraft surfaces, such as thermal and optical coatings, will be the most sensitive to erosion effects because outside the primary beam erosion depths will be measured in in mils. The greatest need for erosion experiments is on nonmetallic targets, but experiments to elucidate the conditions that result in protection of spacecraft surfaces by adsorbed or implanted propellant atoms also are planned.

Very little experimental data exist on the chemical reactions between Hg or Cs and organic spacecraft surfaces. Analysis suggests that Hg^+ will be more troublesome than Hg^0 and that Cs will be of more concern than Hg. Preliminary immersion of six representative spacecraft coatings in Hg and Cs demonstrated significant degradation of H-Film and Teflon FEP by Cs. Beam exposures of these coatings are planned.

The spacecraft metals most likely to undergo important degradation through metallurgical interaction are gold and soft solder with both Cs and Hg. Beam exposures of these metals are planned.

Spacecraft thermal control may be perturbed by thruster material deposition, propellant condensation, changes in surface topography, the implantation of energy within the coating (radiation-type damage), and chemical/metallurgical reactions. Analysis of propellant condensation (assuming the initial existence of a monolayer of condensate) on solar arrays indicates that maximum propellant arrival rates tolerable on the illuminated surface can lead to serious spacecraft design constraints for outward-bound, high-powered vehicles. Literature and experience regarding the other degradation mechanisms are incomplete, but preliminary experiments with Hg^+ beams indicate that white paints will be among the most damage-susceptible surfaces.

Both insulator resistivity and electrode gaps are likely to degrade upon exposure to the propellants. The literature regarding breakdown and high-voltage arcs is adequate for engineering calculations. Insulator resistivity will be studied experimentally.

In conclusion, the designer should make use of tolerance-level criteria for propellant interception by spacecraft surfaces. As yet, firm criteria are not available, but estimates are possible for some problem areas. Thruster material deposition, propellant condensation on the front surfaces of solar arrays, chemical reactions between Cs and nonmetallic materials, ion damage to thermal control coatings, and erosion of thin coatings probably will be the most important effects, but they are unlikely to preclude the use of solar-electric propulsion.

References

[1] Hall, D. F., "Evaluation of Electric Propulsion Beam Divergence and Effects on Spacecraft," 08965-6013-R0-00, Final Report, Contract NAS7-575, Sept. 1969, TRW Systems, Redondo Beach, Calif.

[2] Kemp, R. F., Sellen, J. M., Jr., and Pawlik, E. V., "Neutralizer Tests on a Flight-Model Electron-Bombardment Ion Thrustor," NAS TN D-1733, 1963, NASA.

[3] Milder, N. L., "Comparative Measurements of Singly and Doubly Ionized Mercury Produced by Electron-Bombardment Ion Engine," NAS TN D-1219, 1962, NASA.

[4] Sellen, J. M., Jr., "Investigations of Ion Beam Diagnostics," 8603-6037-SU-000, Contract NAS8-1560, April 1964, TRW Systems, Redondo Beach, Calif.

[5] Hall, D. F., Cho, A. Y., and Shelton, H., "An Experimental Study of Porous Metal Ionizers," AIAA Paper 66-218, San Diego, Calif., 1966.

[6] Reader, P. D., "Durability Tests of Mercury Electron-Bombardment Ion Thrustors," AIAA Paper 66-231, San Diego, Calif., 1966.

[7] Reynolds, T. W. and Richley, E. A., "Propellant Condensation on Surfaces Near an Electric Rocket Exhaust," *Journal of Spacecraft and Rockets*, Vol. 6, No. 10, Oct. 1969, pp. 1155–1161.

[8] Staggs, J. R., Gula, W. P., and Kerslake, W. R., "The Distribution of Neutral Atoms and Charge-Exchange Ions Downstream of an Ion Thruster," *Journal of Spacecraft and Rockets*, Vol. 5, No. 2, Feb. 1968, pp. 159–164.

[9] Magnuson, G. D. et al, "Sputtering Mechanisms Under Ion Propulsion Conditions," GDA-DBE-64-057, Final Report, Contract NAS3-2591, Oct. 1964, General Dynamics/Astronautics, San Diego, Calif.

[10] Langmuir, I., "The Condensation and Evaporation of Gas Molecules," *Collected Works of Irving Langmuir*, Vol. 9, edited by C. G. Suits, Pergamon Press, New York, 1961, p. 72.

[11] Holland, L., "The Growth, Structure and Physical Properties of Vacuum Deposited Films," *Vacuum Deposition of Thin Films*, Wiley, 1958, p. 206.

[12] Holland, L., "The Growth, Structure and Physical Properties of Vacuum Deposited Films," *Vacuum Deposition of Thin Films*, Wiley, New York, 1958, p. 203, 223–235.

[13] Langmuir, I., "The Condensation and Evaporation of Gas Molecules," *Collected Works of Irving Langmuir*, Vol. 9, edited by C. G. Suits, Pergamon Press, New York, 1961, pp. 69–74.

[14] Langmuir, I., "The Evaporation, Condensation, and Reflection of Molecules and the Mechanism of Adsorption," *Collected*

Works of Irving Langmuir, Vol. 9, edited by C. G. Suits, Permagon Press, New York, 1961, p. 42.

[15] Langmuir, I., "The Evaporation, Condensation, and Reflection of Molecules and the Mechanism of Adsorption," *Collected Works of Irving Langmuir*, Vol. 9, edited by C. G. Suits, Permagon Press, New York, 1961, p. 43–46.

[16] Honig, R. E., "Vapor Pressure Data for the Solid and Liquid Elements," *Radio Corporation of America Review*, Vol. 23, No. 4, Dec. 1962, pp. 567–586.

[17] Carter, G. and Colligon, J. S., *Ion Bombardment of Solids*, 1st ed., American Elsevier, New York, 1968, pp. 310–353.

[18] Wehner, G. K., "Influence of the Angle of Incidence on Sputtering Yields," *Journal of Applied Physics*, Vol. 30, No. 11, Nov. 1959, pp. 1762–1765.

[19] Trolinger, J. D., Shipp, J. I., and Lennert, A. E., "Basic Processes of Ion Beam Termination," AEDC-TDR-64-105, Contract AF40(600)-1000, Aug. 1964, ARO Inc.

[20] Szabo, I., "Consecutive Ion-Molecule Reactions in Ethylene Investigated by Means of Positive Ion-Impact," 66-295 DDC AD 63 559, 1966, Air Force Cambridge Research Lab.

[21] "Plastics Properties Chart," *Modern Plastics Encyclopedia*, Vol. 44, No. 1A, McGraw-Hill, New York, 1967, pp. 39–56.

[22] "Propulsion Beam Divergence Effects," First and Second Quarterly Reports, JPL Contract 952350, May and Aug. 1969, TRW Systems, Redondo Beach, Calif.

[23] Kline, G. M., "Permeability of Polymers to Gases, Vapors and Liquids," *Modern Plastics*, Vol. 43, No. 7, March 1966, p. 139.

[24] Keddy, E. S., "Compatibility Evaluation of Materials with Cesium," Rept. LAMS-2948-NASA NG 3-22908, 1963, Los Alamos Scientific Lab.

[25] Stuhlinger, E., ed., *Electric Propulsion Development*, Academic Press, New York, 1963, pp. 348–349.

[26] Slivka, M. J., "A Study of Cesium Vapor Attack on Thermionic Converter Construction Materials," *Advanced Energy Conversion*, Vol. 3, No. 1, March 1963, pp. 157–166.

[27] "Deterioration of Some Aluminum Alloys in the Presence of Mercury and Cesium," Summary Report, Project R3501-B41, Sept. 1962, Armour Research Foundation.

[28] Liebhafsky, H. A., "The Liquidus Curve for Aluminum in Mercury," *Journal of the American Chemical Society*, Vol. 71, No. 4, April 1949, pp. 1468–1470.

[29] Gurinsky, D. H. et al., "Corrision in Liquid Metal Systems," *Proceeding of the 3rd International Conference on Peaceful Uses of Atomic Energy*, United Nations, Vol. 9, New York, 1964, p. 550.

[30] Murphy, A. J., "The Constitution of the Alloys of Silver and Mercury," *Journal of the Institute of Metals*, Vol. 46, 1931, pp. 507–535.

[31] Mendelson, R. A., private communication, Jan., 1968, TRW Systems, One Space Park, Redondo Beach, Calif.

[32] Kienast, G. and Verma, J., "The Behavior of the Alkali Metals Toward Copper, Silver, and Gold," *Zeitschrift fuer Anorganische und Allegemeine Chemie*, Vol. 310, 1961, pp. 143–169.

[33] Hansen, M., *Constitution of Binary Alloys*, 2nd ed., McGraw-Hill, New York, 1958, pp. 207–209.

[34] Holden, R. B., Kells, M. C., and Whitman, C. I., "A Continuous Electrolytic Process for the Preparation of Beryllium Metal," *Proceedings of the 2nd U. N. International Conference on Peaceful Uses of Atomic Energy*, Vol. 4, United Nations, Geneva, 1958, pp. 306–308.

[35] Tipton, C. R., Jr., *Reactor Handbook*, 2nd ed., Vol. 1, Materials Interscience, New York, 1960.

[36] Van Lent, P. H., "The Position of Gray Tin in the Tin-Mercury System," *Acta Metallurgica*, Vol. 9, Feb. 1961, pp. 125–128.

[37] Chandler, W. T. and Hoffman, N. J., "Effects of Liquid Vapor Cesium on Container Metals," TDR-62-965, March 1963, Aeronautical Systems Division of U.S. Air Force.

[38] Hansen, M., *Constitution of Binary Alloys*, 2nd ed., McGraw-Hill, New York, 1958, p. 829.

[39] Parker, W. J. and Abbot, G. C., "Theoretical and Experimental Studies of the Total Emittance of Metals," *Symposium on Thermal Radiation of Solids*, NASA SP-55, 1965, pp. 11–28.

[40] Sklensky, A. F., MacMillan, H. F., and Greenberg, S. A., "Solar-Radiation-Induced Damage to Optical Properties of ZnO-Type Pigments," Technical Summary Report 4-17-68-1, Contact NAS8-18114, Feb. 1968, Lockheed Research Lab., Palo Alto, Calif.

[41] Jorgenson, G. V., "Effects of Simulated Solar-Wind Bombardment on Spacecraft Thermal Control Surfaces," AIAA Paper 65-647, Monterey, Calif., 1965.

[42] Jorgenson, G. V., "Solar-Wind Damage to Spacecraft Thermal Control Coatings," *AIAA Journal*, Vol. 5, No. 6, June 1967, pp. 1204–1205.

[43] Wehner, G. K., "Solar-Wind Bombardment of a Surface in Space," *Symposium on Thermal Radiation of Solids*, SP-55, 1964, NASA, pp. 345–349.

[44] Van Vliet, R. M., *Passive Temperature Control in the Space Environment*, Macmillan, New York, 1965, pp. 210–217, 229–235.

[45] Friichtenicht, J. F. et al, "Study of Micrometeroid Damage to Thermal Control Materials," Final Report, Contract NAS 8-20120, Oct. 1966, TRW Systems, Redondo Beach, Calif.

[46] Hall, D. F., "Propulsion Beam Divergence Effects," Third Quarterly Report, JPL Contract 952350, Nov. 1969, TRW Systems, Redondo Beach, Calif.

[47] Seitz, F., *The Modern Theory of Solids*, McGraw-Hill, New York, 1940, Chap. XVII.

[48] Mott, N. F. and Jones, H., *The Theory of the Properties of Metals and Alloys*, Dover, New York, 1958, pp. 105–125.

[49] Ives, H. and Briggs, H. B., "Optical Constants of Rubidium and Cesium," *Journal of the Optical Society of America*, Vol. 27, 1937, pp. 395–400.

[50] Nathanson, J. B., "The Optical Constants of Solid Cesium," *Physical Review*, Vol. 25, Jan. 1925, pp. 75–84.

[51] "Large Area Solar Array," DZ-113355-7, Final Report-Phase II, JPL Contract 951934, Oct. 1968, Boeing Co., Seattle, Wash.

[52] Barber, T. et al., "1975 Jupiter Flyby Mission Using Solar-Electric Propulsion Spacecraft," Report ASD-760-18, March 1968, Jet Propulsion Lab.

[53] Hass, G. and Hadley, L., "Optical Properties of Metals," *American Institute of Physics Handbook*, edited by D. E. Gray, McGraw-Hill, New York, 1963, pp. 103–121.

[54] Sennett, R. S. and Scott, G. D., "The Structure of Evaporated Metal Films and Their Optical Properties," *Journal of the Optical Society of America*, Vol. 40, No. 4, April 1950, pp. 203–211.

[55] Charbonnier, F. M., Bennette, C. J., and Swanson, L. W., "Electrical Breakdown Between Metal Electrodes in High Vacuum. I. Theory," *Journal of Applied Physics*, Vol. 38, No. 2, Feb. 1967, pp. 627–633.

[56] Bennette, C. J., Swanson, L. W., and Charbonnier, F. M., "Electrical Breakdown Between Metal Electrodes in High Vacuum. II. Experimental," *Journal of Applied Physics*, Vol. 38, No. 2, Feb. 1967, pp. 634–640.

[57] Bennette, C. J. et al., "Investigation of the Prebreakdown Gap Currents Between Clean and Cesium-Coated Tungsten Electrodes," *AIAA Journal*, Vol. 3, No. 2, Feb. 1965, pp. 284–290.